Diffusion Properties and 3D Architecture of Human Lower Leg Muscles Assessed with UHF Strength Diffusion-Tensor MR Imaging and Tractography: Reproducibility and Sensitivity to Sex Difference and Intramuscular Variability[1]

Alexandre Fouré, PhD
Augustin C. Ogier, MSc
Arnaud Le Troter, PhD
Christophe Vilmen, MSc
Thorsten Feiweier, PhD
Maxime Guye, MD, PhD
Julien Gondin, PhD
Pierre Besson, PhD
David Bendahan, PhD

Purpose: To demonstrate the reproducibility of the diffusion properties and three-dimensional structural organization measurements of the lower leg muscles by using diffusion-tensor imaging (DTI) assessed with ultra-high-field-strength (7.0-T) magnetic resonance (MR) imaging and tractography of skeletal muscle fibers. On the basis of robust statistical mapping analyses, this study also aimed at determining the sensitivity of the measurements to sex difference and intramuscular variability.

Materials and Methods: All examinations were performed with ethical review board approval; written informed consent was obtained from all volunteers. Reproducibility of diffusion tensor indexes assessment including eigenvalues, mean diffusivity, and fractional anisotropy (FA) as well as muscle volume and architecture (ie, fiber length and pennation angle) were characterized in lower leg muscles (n = 8). Intramuscular variability and sex differences were characterized in young healthy men and women (n = 10 in each group). Student t test, statistical parametric mapping, correlation coefficients (Spearman rho and Pearson product-moment) and coefficient of variation (CV) were used for statistical data analysis.

Results: High reproducibility of measurements (mean CV ± standard deviation, 4.6% ± 3.8) was determined in diffusion properties and architectural parameters. Significant sex differences were detected in FA (4.2% in women for the entire lower leg; P = .001) and muscle volume (21.7% in men for the entire lower leg; P = .008), whereas architecture parameters were almost identical across sex. Additional differences were found independently of sex in diffusion properties and architecture along several muscles of the lower leg.

Conclusion: The high-spatial-resolution DTI assessed with 7.0-T-MR imaging allows a reproducible assessment of structural organization of superficial and deep muscles, giving indirect information on muscle function.

Online supplemental material is available for this article.

[1] From the Aix-Marseille University, CNRS, Centre de Résonance Magnétique Biologique et Médicale (CRMBM), UMR 7339, Faculté de Médecine la Timone, 27 Boulevard Jean Moulin, 13385 Marseille, France (A.F., A.C.O., A.L.T., C.V., M.G., J.G., P.B., D.B.); APHM, Hôpital Universitaire Timone, CEMEREM, Pôle Imagerie Médicale, Marseille, France (M.G.); Institut NeuroMyoGène, Université Claude Bernard Lyon 1, INSERM U1217, CNRS 5310, Villeurbanne, France (J.G.); and Siemens Healthcare, Erlangen, Germany (T.F.). Received June 13, 2017; revision requested August 8; revision received September 21; accepted September 29; final version accepted October 27. **Address correspondence to** A.F. (e-mail: *alexandre.foure@hotmail.fr*).

Supported by the Agence Nationale pour la Recherche and the French IA Equipex (7T-AMI ANR-11-EQPX-0001, A*MIDEX ANR-11-IDEX-0001-02, A*MIDEX-EI-13-07-130115-08.38-7TAMISTART).

Neuromuscular disorders induce skeletal muscle function impairments (1) related to changes in both muscle volume and structural arrangement of the fascicles and fibers within the muscle, leading to the reduction of skeletal muscle force production (2). The physiologic cross-sectional area (PCSA) is recognized as the most relevant index to estimate the maximal muscle force production capacity (3), but its determination is technically challenging given that information from both muscle volume and architecture are required (4).

Although muscle volume can be accurately measured by using magnetic resonance (MR) imaging (3), muscle architecture parameters (ie, fascicle length and pennation angle) are usually assessed in only two dimensions over a restricted area for relatively superficial skeletal muscles by using B-mode ultrasonography (US) (5). Over the last decade, MR diffusion-tensor imaging (DTI) has been used to characterize muscle architecture in three dimensions and with large volume coverage (6). The diffusion tensor indexes including the principle (λ_1), second (λ_2), and third eigenvalues (λ_3) are used to calculate fractional anisotropy (FA) and mean diffusivity (MD), providing information on muscle diffusion properties and tissue integrity. For instance, altered muscle diffusion properties have been reported as a result of exercise-induced muscle damage (7) and because of neuromuscular diseases (8).

In addition to FA and MD measurements, DTI has been used to track muscle fibers and to assess fiber architecture parameters such as fiber length (L_F) and pennation angle in three dimensions (9,10). Studies have been conducted in several muscle groups such as plantar flexors (9), tibialis anterior (10), and quadriceps femoris muscles (11) but the reproducibility of the corresponding measurements have been scarcely assessed (12,13) and for this limited number of studies, relatively high coefficients of variation (CVs) have been reported (12). It has been suggested that the reproducibility of tractography results could be improved as far as a higher signal-to-noise ratio can be achieved (14); thus, ultra-high-field-strength MR imaging can be considered as a relevant alternative for reproducible diffusion properties and three-dimensional characterization of skeletal muscle architecture.

The aim of our study was to demonstrate the reproducibility of diffusion properties and three-dimensional structural organization measurements of the lower leg muscles by using DTI assessed with ultra-high-field-strength (7.0-T) MR imaging and tractography of skeletal muscle fibers. On the basis of robust statistical mapping analyses, we also aimed at determining the sensitivity of our measurements to sex difference and intramuscular variability.

Materials and Methods

Participants

The reproducibility study was performed with eight young healthy participants: four men (mean age ± standard deviation, 21 years ± 2 [age range, 19–23 years]; mean height, 178 cm ± 5 [height range, 175–185 cm]; mean weight, 67 kg ± 7 [weight range, 57–73 kg]) and four women (mean age, 22 years ± 2 [age range, 20–24 years]; mean height, 164 cm ± 6 [height range, 156–171 cm]; mean weight, 62 kg ± 11 [weight range, 48–73 kg]) underwent two MR imaging sessions. Then, sensitivity of our measurements to sex difference and intramuscular variability was assessed in 20 additional participants: 10 men (mean age, 22 years ± 3 [age range, 18–28 years]; mean height, 174 cm ± 5 [height range, 165–182 cm]; mean weight, 66 kg ± 7 [weight range, 55–76 kg]) and 10 women (mean age, 23 years ± 3 [age range, 19–29 years]; mean height, 165 cm ± 8 [height range, 153–174 cm]; mean weight, 57 kg ± 7 [weight range, 45–70 kg]) underwent a single MR imaging session. Participants with no contraindication to MR imaging (eg, pacemaker, all metallic objects such as implants, claustrophobia), with no affection after interrogation, and with no known musculoskeletal, articular, or cardiovascular dysfunction or abnormalities were included in the study. People staying in a sanitary or social establishment, people in an emergency situation, and pregnant women were excluded from our study. No data have been withdrawn from our study. All 28 participants were recruited between November 2015 and February 2016. Participants were between ages 18 and 30 years and were recreationally active (men, 1.4 hours per week

Implication for Patient Care

- Assessment at once and on a large spatial coverage of all the lower leg muscle volume, diffusion properties, and three-dimensional architecture with 7.0-T MR imaging provides reproducible parameters that might help in diagnosis of muscle tissue alterations leading to muscle function impairments.

https://doi.org/10.1148/radiol.2017171330

Content code: MK

Radiology 2018; 000:1–16

Abbreviations:

ACLL = anterior compartment of lower leg
CV = coefficient of variation
D_F = muscle fiber tract density
DPCLL = deep posterior compartment of lower leg
DTI = diffusion-tensor imaging
FA = fractional anisotropy
LCLL = lateral compartment of lower leg
L_F = fiber length
MD = mean diffusivity
PCSA = physiologic cross-sectional area
SO_{deep} = deep part of soleus
SO_{sup} = superficial part of soleus
SPCLL = superficial posterior compartment of lower leg

Author contributions:

Guarantors of integrity of entire study, A.F., A.L.T., D.B.; study concepts/study design or data acquisition or data analysis/interpretation, all authors; manuscript drafting or manuscript revision for important intellectual content, all authors; approval of final version of submitted manuscript, all authors; agrees to ensure any questions related to the work are appropriately resolved, all authors; literature research, A.F., A.C.O., A.L.T., J.G.; clinical studies, A.F., M.G.; experimental studies, A.F., C.V., J.G., P.B.; statistical analysis, A.F., A.C.O., A.L.T.; and manuscript editing, A.F., A.C.O., A.L.T., J.G., P.B., D.B.

Conflicts of interest are listed at the end of this article.

Figure 1

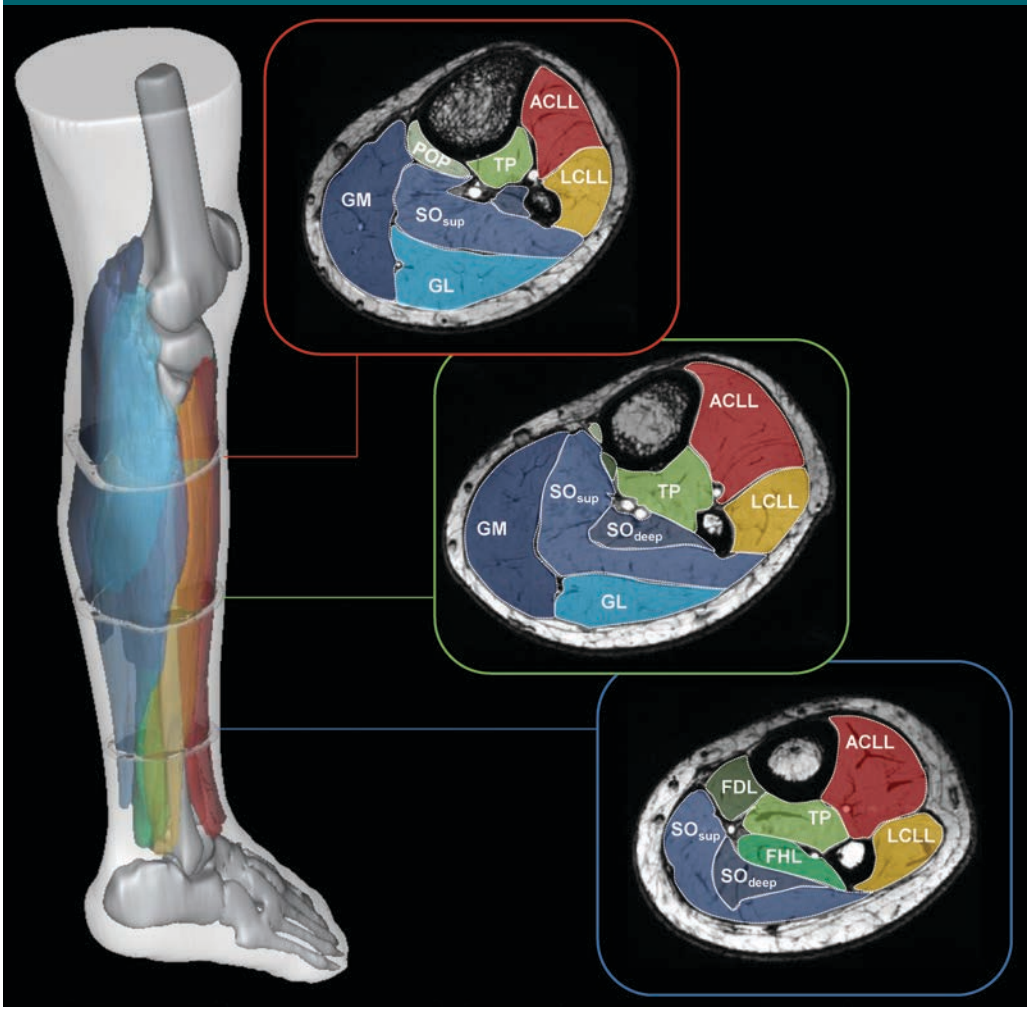

Figure 1: Image shows typical manual delineation of lower leg muscles performed on three different axial sections of T_1-weighted dataset of one male participant. Four compartments of lower leg were delineated on T_1-weighted images including superficial posterior compartment of lower leg (SPCLL) composed of gastrocnemius lateralis (GL), gastrocnemius medialis (GM), deep part of soleus (SO_{deep}), and superficial part of soleus (SO_{sup}); deep posterior compartment of lower leg (DPCLL) composed of flexor hallucis longus (FHL), flexor digitorum longus (FDL), tibialis posterior (TP), and popliteus (POP); muscles of anterior compartment of lower leg (ACLL) and lateral compartment of lower leg (LCLL) (ACLL includes extensor digitorum longus, extensor hallucis longus, tibialis anterior, and fibularis tertius; LCLL includes fibularis longus and fibularis brevis).

± 1.1; women, 1.2 hours per week ± 1.1) but none of them were engaged in any training or exercise programs. Participants were instructed to avoid any intense or unaccustomed physical activities, to keep their dietary habits, and to avoid smoking and consuming caffeine, medicine, and alcohol during the week before the experiment. The number of participants to be assessed regarding sex differences (n = 10 in each group) was determined on the basis of a statistical power calculation (α = .05 and $1-\beta$ = .8) and previous studies (15,16) to detect a significant sex difference of 10% in the mean FA of the gastrocnemius lateralis muscle and 8.5% in the pennation angle of the superficial part of the soleus muscle (SO_{sup}). Our prospective study was approved by the local human research ethics committee *Sud Mediterranée I* (2015-A00121–48), and was conducted in compliance with the Declaration of Helsinki. Our study was referenced on *https://clinicaltrials.gov* (NCT02402751). Volunteers were fully informed about the nature and the aim of the study and gave their written informed consent to participate. D.B. and M.G. had control of the data. T.F. is employed by Siemens Healthcare and holds patents related to the improvement of image quality and acquisition speed of MR diffusion imaging. None of them has an exclusive connection to

Figure 2

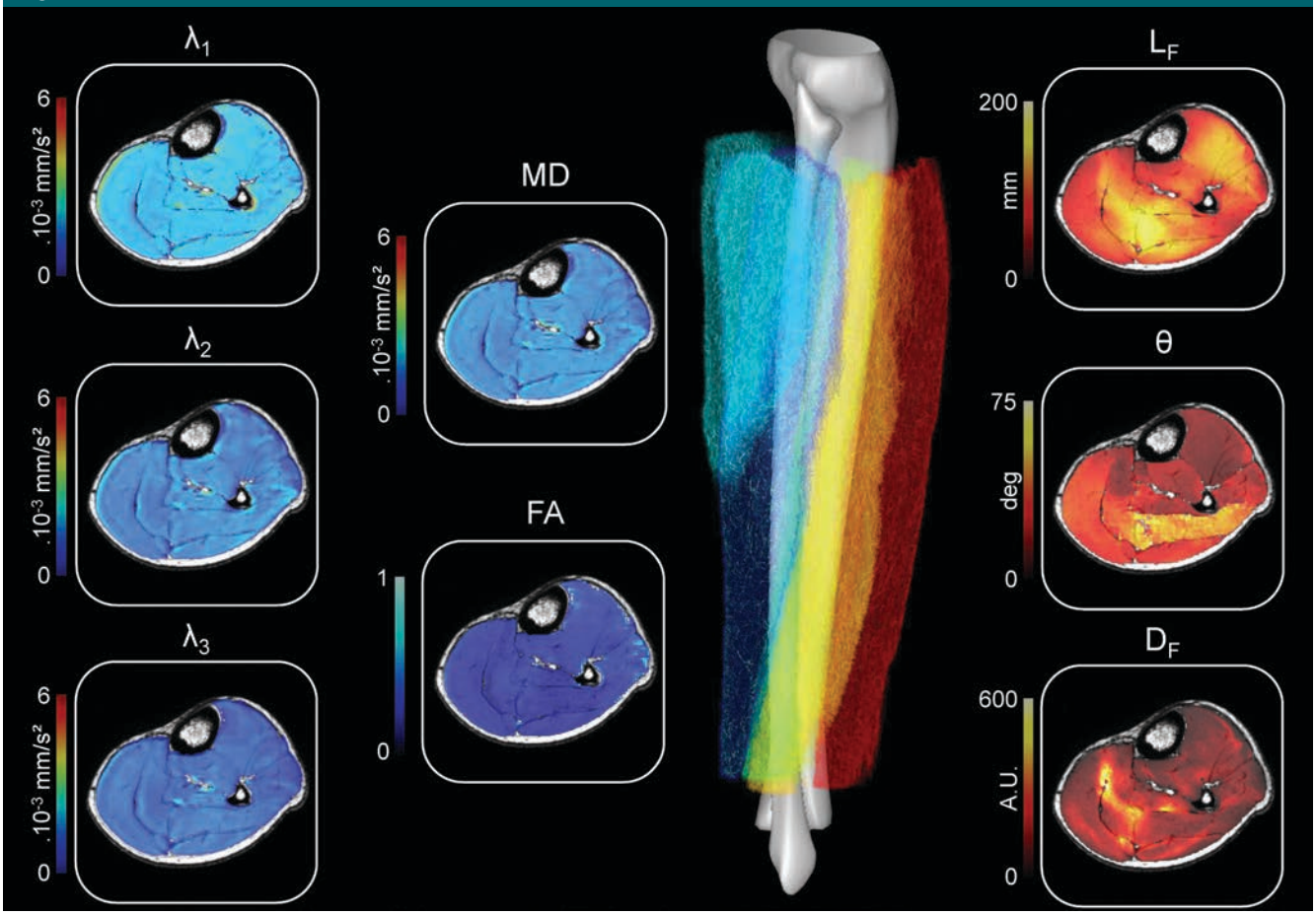

Figure 2: Maps show λ_1, λ_2, λ_3, mean diffusivity (MD), and fractional anisotropy (FA) as well as architecture parameters (fiber length [L_F], pennation angle [θ], and muscle fiber tract density [D_F]) related to muscle fibers tractography result represented in three dimensions.

muscle diffusion imaging or the evaluation of corresponding data. No patent is directly linked to the article.

For both reproducibility and sensitivity tests, muscle diffusion properties and three-dimensional architecture parameters were assessed. Measurements were performed in the proximal part of the right lower leg for the reproducibility study and in the whole muscles for the sensitivity assessment.

Data Acquisition

Participants were positioned supine in a 7.0-T whole-body research imager (Siemens Healthcare, Erlangen, Germany). A 28-channel proton knee coil was used for imaging of the right lower leg muscles. While the leg was fully extended, the foot was maintained in a fixed position at 15°–20° in plantar flexion (0° is neutral position with foot perpendicular to the tibia) to ensure that no passive tension occurred in lower leg muscles. Localized B_0 shimming was performed with second-order shims by using the vendor's product interactive shim program. Volume of lower leg muscles was determined from high-spatial-resolution T_1-weighted images. Axial multidirectional diffusion-weighted images were acquired with a standard "monopolar" Stejskal-Tanner diffusion encoding scheme–that is, a single spin-echo refocusing (17). Standard chemically selective fat suppression was used and a prototype sequence providing a gradient-reversal technique was added to improve the saturation efficiency (18). Data were acquired from two stacks (ie, proximal and distal parts) in two opposite phase-encoding polarities to correct for distortions (19). The total imaging time was 48 minutes 44 seconds. MR imaging sequence parameters are reported in Table E1 (online).

Data Analysis

Muscle segmentation.—Regions of interest were manually drawn on T_1-weighted images by an experienced researcher (A.F., with 8 years of experience in muscle anatomy and geometry assessment) by using FSLView version 3.2.0 (FSL, FMRIB Software Library, Oxford, UK) as displayed in Figure 1 . Muscle areas were segmented every

Figure 3

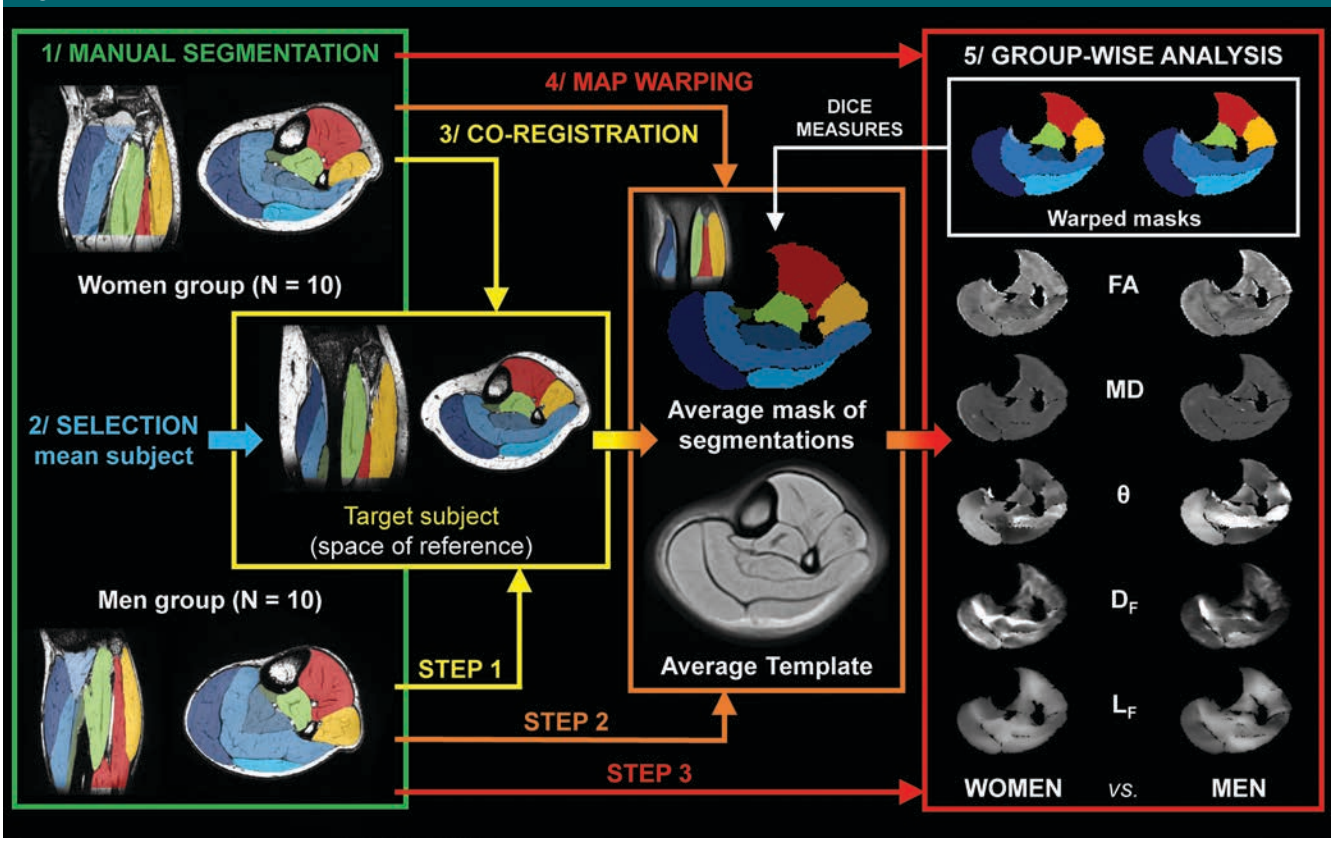

Figure 3: Flowchart of preprocessing steps required to spatially normalize T_1-weighted images with initial intersubject affine coregistration and additional nonlinear coregistration performed on segmentations masks (Step 1 and 2). Quality of coregistrations was assessed by using Dice similarity coefficients. Registration fields were then applied to diffusion tensor imaging (DTI)–derived maps (Step 3). D_F = muscle fiber tract density, FA = fractional anisotropy, L_F = fiber length, MD = mean diffusivity, θ = pennation angle.

five slices and missing slices were automatically interpolated (20) (for details, see Appendix E1 [online]). Muscle volume was calculated by summing the volume of each muscle in all the slices. Nonmuscle volume (eg, blood vessels, intramuscular fat) was excluded from analysis.

Correction of diffusion-weighted images.—The pipeline of data processing is displayed in Figure E1 (online). Each diffusion-weighted dataset was denoised by using BM4D algorithm (21). Geometric and signal distortions associated to echo planar imaging were estimated on b = 0 sec/mm^2 images with the *topup* function from FSL software, and modifications were applied to correct images from these distortions and Eddy currents by using FSL *eddy* function. Intensity of nondistorted diffusion- and T_1-weighted images were corrected from B_1 homogeneities by using *N4ITK* algorithm from *ANTs* library (22). Finally, each T_1-weighted image was registered with the corresponding image obtained for b = 0 sec/mm^2 by using three-dimensional rigid body transformation, subsequently applied to muscle segmentation masks.

Muscle diffusion properties and tractography parametrization.—Diffusion tensors were fitted at each voxel to calculate FA and MD maps with the MRtrix software package (version 3; Brain Research Institute, Melbourne, Australia; *http://www.mrtrix.org*). Distribution of DTI-derived parameters (ie, eigenvalues, MD, and FA) and potential changes along muscle were assessed. Muscle fiber tracking was done by using the binarized segmentation mask of the whole lower leg muscles with the MRtrix software package. Tracking parameters were adapted from previously reported criteria (10) applied to initiate or stop muscle fiber tractography. The algorithm generated 2 000 000 fiber tracts with length ranging from 5 mm to 200 mm. All voxels in the binarized segmentation mask were used as seeds, and the tracking procedure was stopped if a fiber tract reached a voxel outside the mask of each muscle or if a stopping criterion was met (see Appendix E1 [online]).

Three-dimensional muscle architecture and fiber tract density mapping.—From muscle fiber tractography (Fig 2), muscle L_F, and pennation angle were

Table 1

Reproducibility of Diffusion Tensor Indexes and Muscle Architecture Parameters

Muscle and Parameter	Test No. 1	Test No. 2	Standard Error of Measurement	Coefficient of Variation (%)
Gastrocnemius lateralis				
Volume (cm^3)	66 ± 26	63 ± 22	4	5.6
FA	0.225 ± 0.011	0.225 ± 0.017	0.01	5.1
MD ($\times 10^{-3}$ mm^2/sec)	1.597 ± 0.058	1.595 ± 0.028	0.04	2.5
L_F (mm)	55 ± 10	54 ± 7	3	5.6
θ (degrees)	25 ± 4	24 ± 5	3	13.8
Gastrocnemius medialis				
Volume (cm^3)	132 ± 29	128 ± 29	3	3.3
FA	0.219 ± 0.014	0.211 ± 0.011	0.01	4.1
MD ($\times 10^{-3}$ mm^2/sec)	1.565 ± 0.034	1.549 ± 0.041	0.03	1.5
L_F (mm)	54 ± 5	51 ± 6	3	5.5
θ (degrees)	34 ± 4	34 ± 2	3	8.9
Soleus				
Superficial				
Volume (cm^3)	204 ± 35	200 ± 32	4	2.0
FA	0.212 ± 0.017	0.208 ± 0.016	0.01	2.7
MD ($\times 10^{-3}$ mm^2/sec)	1.571 ± 0.053	1.574 ± 0.032	0.03	1.8
L_F (mm)	38 ± 5	39 ± 4	1	2.8
θ (degrees)	43 ± 3	42 ± 4	2	5.5
Deep				
Volume (cm^3)	50 ± 19	48 ± 18	2	4.5
FA	0.218 ± 0.014	0.219 ± 0.012	0.01	4.6
MD ($\times 10^{-3}$ mm^2/sec)	1.607 ± 0.044	1.587 ± 0.043	0.01	0.8
L_F (mm)	41 ± 9	40 ± 9	2	3.5
θ (degrees)	29 ± 6	28 ± 6	2	6.6
Superficial posterior compartment of lower leg				
Volume (cm^3)	453 ± 75	439 ± 73	7	1.8
FA	0.271 ± 0.020	0.268 ± 0.016	0.01	3.8
MD ($\times 10^{-3}$ mm^2/sec)	1.642 ± 0.041	1.629 ± 0.028	0.04	2.2
L_F (mm)	47 ± 3	46 ± 3	1	1.9
θ (degrees)	33 ± 2	32 ± 3	1	5.1
Flexor hallucis longus				
Volume (cm^3)	3 ± 4	3 ± 4	0.3	17.1
FA	0.297 ± 0.042	0.288 ± 0.043	0.04	16.4
MD ($\times 10^{-3}$ mm^2/sec)	1.735 ± 0.068	1.727 ± 0.135	0.12	7.4
L_F (mm)	18 ± 6	18 ± 6	1	6.5
θ (degrees)	25 ± 8	22 ± 3	3	22.1
Flexor digitorum longus				
Volume (cm^3)	7 ± 3	7 ± 2	0.3	5.2
FA	0.264 ± 0.019	0.260 ± 0.012	0.01	5.0
MD ($\times 10^{-3}$ mm^2/sec)	1.600 ± 0.056	1.582 ± 0.065	0.04	2.4
L_F (mm)	25 ± 3	26 ± 3	2	9.5
θ (degrees)	21 ± 5	19 ± 3	3	9.6
Tibialis posterior				
Volume (cm^3)	47 ± 13	46 ± 12	1	2.7
FA	0.260 ± 0.014	0.257 ± 0.014	0.01	1.0
MD ($\times 10^{-3}$ mm^2/sec)	1.667 ± 0.032	1.652 ± 0.042	0.02	1.0
L_F (mm)	48 ± 9	47 ± 7	3	8.1
θ (degrees)	24 ± 3	24 ± 3	2	7.6

Table 1 (continues)

characterized. Pennation angle was determined as the angle between the principal axis of the muscle (determined from a principal component analysis on the three-dimensional coordinates of each muscle segmentation mask) and the global direction of each fiber tracked within the muscle (determined as the direction between the first and the last fiber tract points within the muscle). L_F and pennation angle were averaged over all fiber tracts within each voxel (23). Histograms representing the number of voxels with respect to L_F (range, 5–200 mm) and pennation angle (range, 0°–90°) were also determined for each muscle of the lower leg.

As previously described (4), the PCSA was calculated by using the following equation:

$$\mathrm{PCSA} = \frac{V_M}{L_F} \times \cos\theta,$$

where V_M is the muscle volume and θ is the pennation angle. Muscle fiber tract density (D_F) was mapped in each muscle and compartment of the lower leg (23).

Sex difference and intramuscular variability.—Additional analyses were performed by using three-dimensional spatial normalization and statistical parametric mapping to assess and localize sex difference in maps of FA, MD, L_F, pennation angle, and D_F for men and women on the basis of an original methodology (Fig 3) as previously described (24). Dice similarity coefficients were used to estimate the quality of image coregistration (see Appendix E1 [online]). On the basis of coregistrated images of the lower leg muscles associated to three-dimensional spatial normalization, each muscle volume was divided in three equal parts (ie, distal, central, and proximal) to discriminate potential changes in diffusion properties and architecture parameters along muscle and across sex. Quantitative data for reproducibility analysis and sex difference assessment were extracted before the intersubject registration of images. The three-dimensional normalization of images was performed to localize sex differences with statistical parametric

Table 1 *(continued)*

Muscle and Parameter	Test No. 1	Test No. 2	Standard Error of Measurement	Coefficient of Variation (%)
Popliteus				
Volume (cm^3)	9 ± 3	8 ± 3	1	8.4
FA	0.263 ± 0.027	0.267 ± 0.039	0.01	4.6
MD ($\times 10^{-3}$ mm^2/sec)	1.567 ± 0.074	1.555 ± 0.059	0.06	4.0
L_F (mm)	19 ± 2	19 ± 2	1	3.2
θ (degrees)	39 ± 7	38 ± 6	4	12.8
Deep posterior compartment of lower leg				
Volume (cm^3)	66 ± 19	63 ± 18	2	2.9
FA	0.219 ± 0.009	0.216 ± 0.010	0.05	2.4
MD ($\times 10^{-3}$ mm^2/sec)	1.585 ± 0.031	1.576 ± 0.022	0.02	1.0
L_F (mm)	26 ± 4	26 ± 5	1	4.4
θ (degrees)	25 ± 4	24 ± 4	1	3.7
Lateral compartment of lower leg				
Volume (cm^3)	61 ± 16	60 ± 15	1	2.9
FA	0.278 ± 0.023	0.271 ± 0.018	0.01	3.9
MD ($\times 10^{-3}$ mm^2/sec)	1.707 ± 0.054	1.705 ± 0.074	0.05	1.6
L_F (mm)	53 ± 5	52 ± 9	4	9.4
θ (degrees)	30 ± 4	29 ± 4	4	14.2
Anterior compartment of lower leg				
Volume (cm^3)	116 ± 36	114 ± 33	3	3.2
FA	0.279 ± 0.019	0.271 ± 0.015	0.01	3.5
MD ($\times 10^{-3}$ mm^2/sec)	1.648 ± 0.046	1.657 ± 0.070	0.04	2.9
L_F (mm)	81 ± 8	82 ± 8	3	4.4
θ (degrees)	19 ± 3	17 ± 3	1	8.4

Note.—Unless otherwise noted, data are means ± standard deviation. FA is unitless. FA = fractional anisotropy, L_F = fiber length, MD = mean diffusivity, θ = pennation angle.

mapping analysis and to assess intramuscular variabilities.

Maximal Voluntary Isometric Contraction Torque

Muscle force was calculated from the external torque measured during an isometric plantar flexion and the muscle moment arm length in men and women (see Appendix E1 [online]).

Statistics

The distribution of data was checked by using the Shapiro-Wilk tests (Table E2 [online]) and parametric statistical tests were performed by using Statistica software (version 10; Statsoft, Tulsa, OK). For the reproducibility measurements, CV and standard error of measurement were quantified. Reproducibility was considered as good for CV less than 10% on the basis of a previous report (25). Sex differences were assessed by using Student *t* test and statistical parametric mapping analysis, whereas correlations between muscle force and geometric parameters were assessed by using Pearson product-moment correlation (*r*) and Spearman rank correlation (ρ) coefficients (see Appendix E1 [online]). Intramuscular variabilities were assessed with a two-way analysis of variance (parts [distal, central, proximal] and sex [male or female] factors) and a Tukey honest significant difference post hoc analysis was performed when appropriate. The level of significance was set at $P < .05$.

Results

Reproducibility

Considering the low CVs and standard error of measurements, a high reproducibility of the diffusion properties and architectural parameters (mean CV, 3.2% ± 2.6 [range, 0.8%–16.4%] and mean CV, 8.4% ± 4.6 [range, 2.8%–22.1%], respectively) was found in lower leg muscles (Table 1). The reproducibility of D_F was good with a mean CV of 3.0% considering all muscles of the lower leg (superficial posterior compartment of the lower leg [SPCLL], 3.7%; deep posterior compartment of the lower leg [DPCLL], 12.1%; lateral compartment of the lower leg [LCLL], 12.2%; and anterior compartment of the lower leg [ACLL], 8.6%). The reproducibility of PCSA calculations was also good considering all muscles of the lower leg with a mean CV of 5.2% ± 2.0 (range, 2.5%–8.9%) and a low standard error of measurement (mean, 0.5 cm^2 ± 0.4 [range, 0.13–1.39 cm^2]).

Sex Difference and Intramuscular Variability

Considering the whole set of muscles from the lower leg, FA was 4.2% higher for women compared with men (P = .001; Table 2). As shown in Figure 4, a rightward shift in the relationships between the relative muscle volume and the voxel FA value was observed in most of the lower leg muscles for women compared with men. In contrast, the distribution of MD, λ_1, λ_2 and λ_3 values relative to muscle volume was similar in young healthy men and women (Fig 4, Fig E2 [online]).

The distribution of L_F and pennation angle reported in Figure 5 illustrates a slight sex difference in muscle architecture for the lower leg of healthy men and women. Significant sex differences were only found in L_F of all DPCLL muscles (ie, L_F for men > L_F for women for flexor hallucis longus, flexor digitorum longus, tibialis posterior, and popliteus) and pennation angle of flexor digitorum longus (Table 3). A significantly higher D_F value was found for women compared with men (Table 3) in SPCLL (15.6%; P = .011), LCLL (19.4%; P = .036), and ACLL (16.0%; P = .003).

In contrast, a significantly higher whole lower leg muscle volume (21.7%) was characterized for men compared

Table 2

Diffusion Properties Parameters Assessed from DTI in Each Muscle of the Lower Leg for Men and Women

Muscle	Men					Women				
	FA	MD	λ_1	λ_2	λ_3	FA	MD	λ_1	λ_2	λ_3
Gastrocnemius lateralis	0.221 ± 0.015	1.554 ± 0.038	1.933 ± 0.062	1.460 ± 0.038	1.268 ± 0.032	0.243 ± 0.017*	1.581 ± 0.054	2.005 ± 0.054*	1.483 ± 0.075	1.256 ± 0.046
Gastrocnemius medialis	0.216 ± 0.014	1.530 ± 0.035	1.897 ± 0.054	1.447 ± 0.038	1.244 ± 0.032	0.222 ± 0.012	1.551 ± 0.051	1.938 ± 0.066	1.476 ± 0.048	1.239 ± 0.057
Soleus										
Superficial	0.205 ± 0.011	1.540 ± 0.035	1.886 ± 0.051	1.471 ± 0.034	1.263 ± 0.031	0.206 ± 0.012	1.565 ± 0.037	1.916 ± 0.038	1.506 ± 0.044	1.274 ± 0.041
Deep	0.210 ± 0.009	1.597 ± 0.043	1.960 ± 0.066	1.530 ± 0.040	1.301 ± 0.030	0.216 ± 0.012	1.601 ± 0.057	1.976 ± 0.089	1.531 ± 0.056	1.296 ± 0.051
Superficial posterior compartment of lower leg	0.212 ± 0.008	1.555 ± 0.031	1.915 ± 0.043	1.479 ± 0.031	1.269 ± 0.024	0.218 ± 0.008	1.574 ± 0.037	1.950 ± 0.041	1.502 ± 0.044	1.269 ± 0.034
Flexor hallucis longus	0.245 ± 0.008	1.637 ± 0.062	2.080 ± 0.082	1.562 ± 0.065	1.269 ± 0.045	0.258 ± 0.014*	1.645 ± 0.036	2.111 ± 0.052	1.566 ± 0.033	1.257 ± 0.041
Flexor digitorum longus	0.264 ± 0.015	1.489 ± 0.170	1.919 ± 0.190	1.432 ± 0.170	1.117 ± 0.156	0.279 ± 0.016*	1.509 ± 0.266	1.993 ± 0.295	1.437 ± 0.269	1.097 ± 0.239
Tibialis posterior	0.268 ± 0.019	1.451 ± 0.191	1.900 ± 0.187	1.361 ± 0.194	1.092 ± 0.195	0.277 ± 0.017	1.591 ± 0.052*	2.096 ± 0.069*	1.486 ± 0.056	1.192 ± 0.064
Popliteus	0.268 ± 0.023	1.534 ± 0.065	1.974 ± 0.085	1.473 ± 0.073	1.154 ± 0.066	0.294 ± 0.019*	1.534 ± 0.065	2.021 ± 0.099	1.486 ± 0.095	1.118 ± 0.069
Deep posterior compartment of lower leg	0.262 ± 0.012	1.513 ± 0.121	1.955 ± 0.126	1.440 ± 0.123	1.146 ± 0.118	0.275 ± 0.010*	1.573 ± 0.090	2.061 ± 0.107	1.489 ± 0.093	1.170 ± 0.077
Lateral compartment of lower leg	0.267 ± 0.011	1.632 ± 0.084	2.095 ± 0.106	1.588 ± 0.080	1.212 ± 0.072	0.280 ± 0.016*	1.632 ± 0.084	2.174 ± 0.107	1.613 ± 0.084	1.218 ± 0.065
Anterior compartment of lower leg	0.270 ± 0.010	1.545 ± 0.056	2.000 ± 0.060	1.481 ± 0.065	1.155 ± 0.050	0.283 ± 0.007*	1.545 ± 0.056	2.079 ± 0.104	1.513 ± 0.069	1.169 ± 0.068
All muscles	0.245 ± 0.006	1.549 ± 0.055	1.964 ± 0.061	1.480 ± 0.056	1.202 ± 0.051	0.255 ± 0.005*	1.589 ± 0.057	2.037 ± 0.072*	1.514 ± 0.055	1.215 ± 0.048

Note.—Data are means ± standard deviation. Unless otherwise noted, data are given as $\times 10^{-3}$ mm^2/sec. FA is unitless. FA = fractional anisotropy, MD = mean diffusivity.

* Significantly different from men ($P < .05$).

with women (Table 3). A significant difference was found considering all plantar flexor muscles including SPCLL and DPCLL (20.2% for men compared with women; $P = .025$) and the dorsi flexors muscles included in ACLL ($P = .003$; Table 3). Men also exhibited higher PCSA for the ACLL (mean PCSA, 21 cm^2 ± 3 vs mean PCSA, 26 cm^2 ± 2; $P = .001$), SPCLL, and DPCLL compared with women (Table 4). The relative contribution of each muscle in the total lower leg muscle volume and PCSA is reported in Table E3 (online).

The Dice similarity coefficients associated to the coregistration of images, masks, and quantitative maps were very high for all the lower leg muscles (0.91 ± 0.04 [range, 0.65–0.96]). Statistical parametric mapping analysis revealed only few significant local differences regarding sex (Fig E3 [online]). Main differences were found for FA in the proximal part of ACLL, SO_{sup}, the distal part of LCLL and for D_F in the gastrocnemius medialis, the proximal part of ACLL, LCLL, and SO_{sup}.

Box plots displayed additional differences independently of sex along several muscles of the lower leg (Figs 6, 7). For instance, FA was higher in the proximal part of the gastrocnemius medialis and the deep part of the soleus (SO_{deep}) compared with the central and distal parts. MD was also higher in the proximal part for tibialis posterior, whereas it was higher in the distal part for LCLL and gastrocnemius lateralis (Fig 6). L_F was significantly higher in the central part for gastrocnemius lateralis, flexor hallucis longus, and popliteus but lower in the distal part for gastrocnemius medialis, SO_{sup}, flexor hallucis longus, LCLL, and ACLL. Pennation angle was lower in proximal part of SO_{sup}, tibialis posterior, and ACLL (Fig 7).

Muscle force production capacity.—The torque during maximal voluntary isometric contraction was significantly greater in men compared with women (38.8%; $P = .001$; Table 4). Despite a smaller muscle moment arm of 6.1% in women ($P = .005$), muscle force was still greater in men compared with women (30.6%; $P = .001$; Table 4).

Figure 4

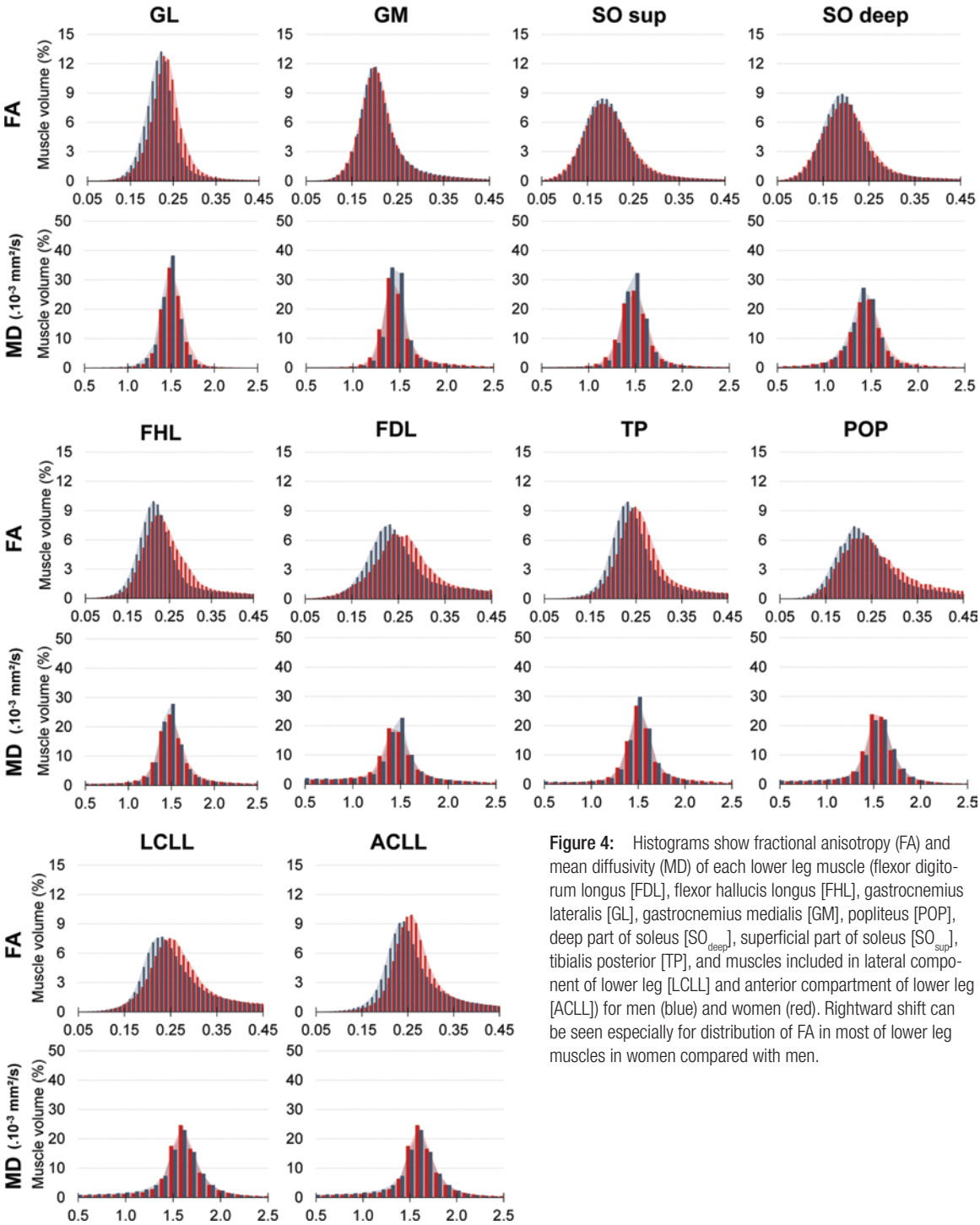

Figure 4: Histograms show fractional anisotropy (FA) and mean diffusivity (MD) of each lower leg muscle (flexor digitorum longus [FDL], flexor hallucis longus [FHL], gastrocnemius lateralis [GL], gastrocnemius medialis [GM], popliteus [POP], deep part of soleus [SO_{deep}], superficial part of soleus [SO_{sup}], tibialis posterior [TP], and muscles included in lateral component of lower leg [LCLL] and anterior compartment of lower leg [ACLL]) for men (blue) and women (red). Rightward shift can be seen especially for distribution of FA in most of lower leg muscles in women compared with men.

Correlations.—Significant correlation (r = 0.52; P = .02 but ρ = 0.38; P = .10) was found between maximal muscle force capacity and SPCLL volume (Fig E4 [online]). However, higher correlation coefficients (ie, especially the ρ coefficient) were found (r = 0.59; P = .01 and ρ = 0.56; P = .01) between force and PCSA of SPCLL muscles (Fig 8).

Figure 5

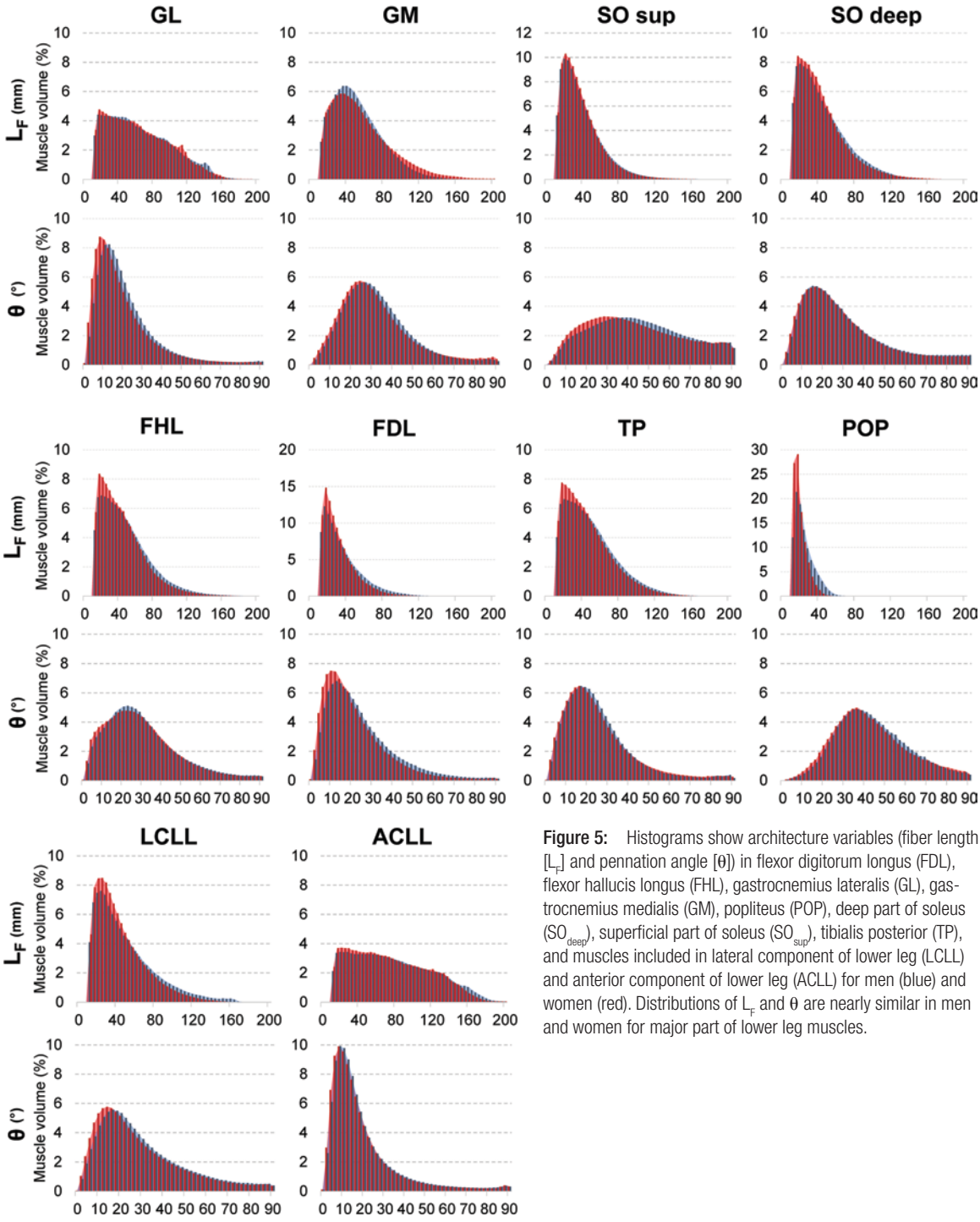

Figure 5: Histograms show architecture variables (fiber length [L_F] and pennation angle [θ]) in flexor digitorum longus (FDL), flexor hallucis longus (FHL), gastrocnemius lateralis (GL), gastrocnemius medialis (GM), popliteus (POP), deep part of soleus (SO_{deep}), superficial part of soleus (SO_{sup}), tibialis posterior (TP), and muscles included in lateral component of lower leg (LCLL) and anterior component of lower leg (ACLL) for men (blue) and women (red). Distributions of L_F and θ are nearly similar in men and women for major part of lower leg muscles.

Discussion

Our study demonstrated that ultra-high-field-strength MR imaging allows a reproducible assessment of diffusion properties and three-dimensional architecture of lower leg muscles from high-spatial-resolution DTI with a large volume coverage even for deep muscles. Only slight sex differences were found in muscle tissue FA, L_F, and pennation angle of young healthy participants.

Table 3

Volume and Architectural Parameters Assessed from Fiber Tractography in Each Muscle of the Lower Leg for Men and Women

Muscle	Volume (cm^3)			L_F (mm)			θ (degree)			D_F (tracts/voxel)		
	Men	Women	*P* Value	Men	Women	*P* Value	Men	Women	*P* Value	Men	Women	*P* Value
Gastrocnemius lateralis	84 ± 23	66 ± 12*	.038	61 ± 12	62 ± 8	.879	20 ± 5	20 ± 3	.635	144 ± 23	159 ± 33	.256
Gastrocnemius medialis	145 ± 30	136 ± 30	.507	50 ± 5	54 ± 7	.233	32 ± 4	31 ± 2	.576	122 ± 23	157 ± 25*	.004
Soleus												
Superficial	290 ± 58	250 ± 50	.110	37 ± 6	36 ± 4	.765	44 ± 3	42 ± 3	.398	216 ± 34	247 ± 29*	.037
Deep	76 ± 23	65 ± 26	.297	42 ± 5	39 ± 7	.365	31 ± 4	29 ± 5	.350	166 ± 20	185 ± 21*	.046
Superficial posterior compartment of lower leg	596 ± 114	517 ± 97	.108	47 ± 5	48 ± 5	.917	32 ± 3	31 ± 2	.324	162 ± 18	187 ± 21*	.011
Flexor hallucis longus	54 ± 9	42 ± 11*	.014	46 ± 4	41 ± 6*	.023	29 ± 4	29 ± 4	.866	242 ± 50	232 ± 40	.604
Flexor digitorum longus	27 ± 4	18 ± 5*	.001	33 ± 4	29 ± 4*	.030	23 ± 4	20 ± 3*	.034	103 ± 20	107 ± 27	.716
Tibialis posterior	97 ± 16	73 ± 20*	.009	47 ± 3	43 ± 4*	.047	24 ± 3	24 ± 2	.825	108 ± 16	119 ± 16	.147
Popliteus	15 ± 5	8 ± 2*	.001	21 ± 3	17 ± 2*	.001	44 ± 6	44 ± 8	.875	48 ± 11	43 ± 14	.325
Deep posterior compartment of lower leg	193 ± 24	141 ± 29*	.001	37 ± 1	32 ± 2*	.001	30 ± 3	29 ± 2	.547	125 ± 18	125 ± 18	.096
Superficial posterior + deep posterior compartment of lower leg	790 ± 125	657 ± 117*	.025	42 ± 3	40 ± 3	.143	31 ± 3	30 ± 2	.331	144 ± 19	156 ± 17	.077
Lateral compartment of lower leg	117 ± 25	94 ± 14*	.021	46 ± 9	42 ± 3	.167	29 ± 2	28 ± 3	.156	95 ± 21	113 ± 15*	.036
Anterior compartment of lower leg	220 ± 28	175 ± 32*	.003	76 ± 6	73 ± 6	.257	19 ± 1	18 ± 3	.578	120 ± 13	139 ± 12*	.003

Note.—Unless otherwise noted, data are means ± standard deviation. D_F = fiber tract density, L_F = fiber length, θ = pennation angle.

* Significantly different from men.

However, intramuscular differences in diffusion properties and architecture along muscles have been highlighted independently of sex by using three-dimensional spatial normalization of images and statistical parametric mapping analysis. Interestingly, maximal muscle force production of plantar flexor muscles was positively correlated with the PCSA, suggesting that DTI measurements can be used to noninvasively assess maximum voluntary muscle force production capacity in vivo.

Reproducibility of DTI-derived variables was generally good for diffusion properties and three-dimensional muscle architecture variables assessed in our study compared with what has been previously reported by using MR imaging at lower field strength (eg, 12). Although the architecture measurements reported in our study for the superficial muscles were more variable than those reported by using US (5,26), this apparent difference might be related to the fact that DTI allows a three-dimensional assessment of muscle architecture with larger muscle volume coverage. This larger muscle coverage allows the assessment of deep muscles and might also be more representative of the whole muscle volume compared with US measurements. Overall, the absolute values of L_F, pennation angle, and PCSA were in accordance with those reported in previous studies in superficial muscles such as gastrocnemii (9,27). Data obtained in deep muscles were also in the range of values described in cadaver studies despite a small sample size in these latter studies (eg, 28). It is noteworthy that the pennation angle was determined between the fiber tract direction and the principal axis of the whole muscle in our study, whereas angle between the directions of the fascicles and the local muscle aponeurosis are usually reported (6,9), which can lead to potential discrepancies with results of previous studies. Furthermore, D_F appears as a reproducible and noninvasive parameter that can potentially be used to indirectly assess relative geometry of muscle fibers and fascicles (ie, cross-sectional area).

Figure 6

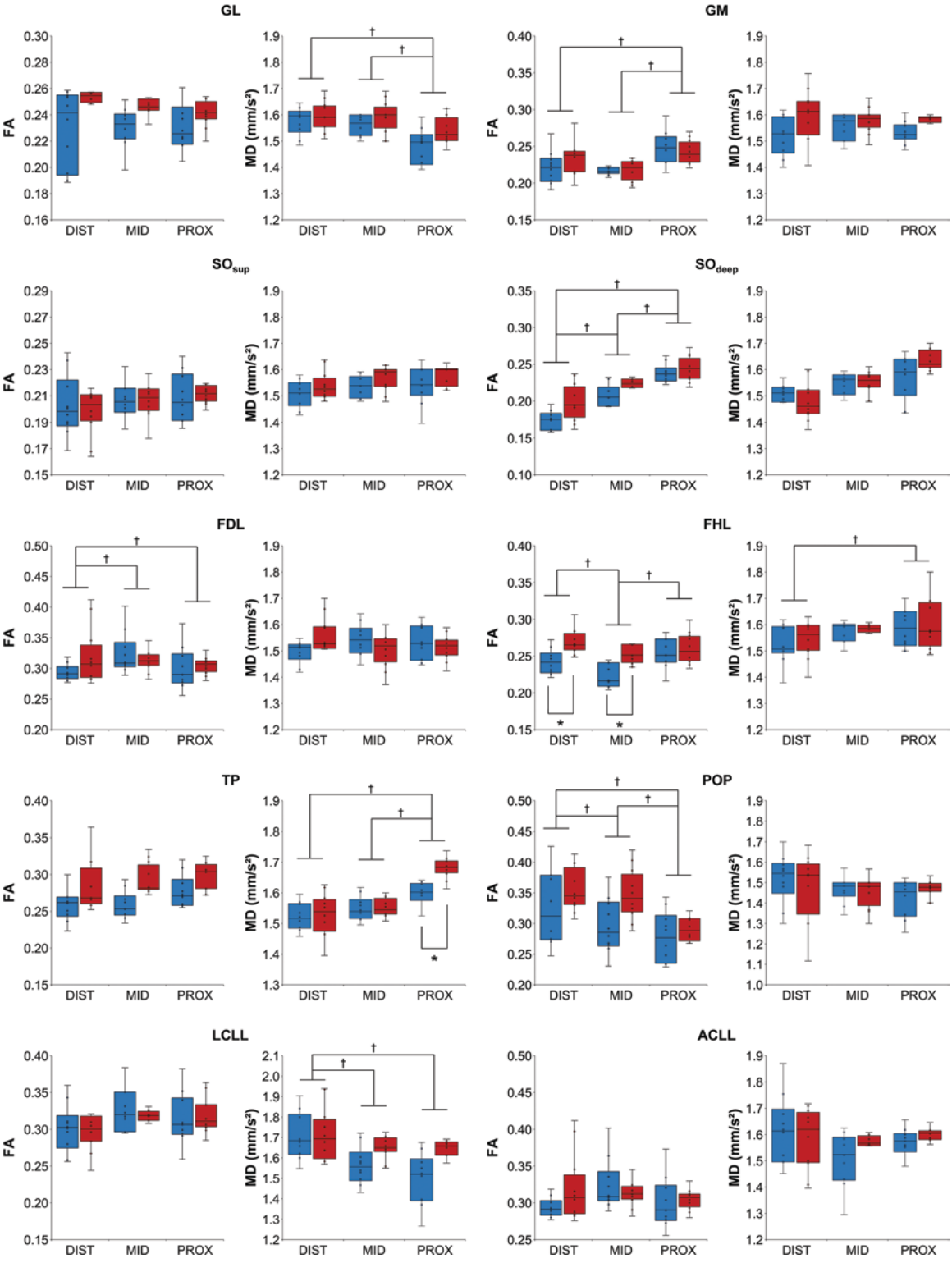
GL
GM
SO$_{sup}$
SO$_{deep}$
FDL
FHL
TP
POP
LCLL
ACLL
FA
MD (mm/s²)
DIST
MID
PROX

Table 4

Muscle PCSA and Maximal Voluntary Plantar Flexion Force Capacity Assessed in Men and Women

Parameter and Muscle	Men ($n = 10$)	Women ($n = 10$)	*P* Value
PCSA (cm^2)			
Gastrocnemius lateralis	12 ± 2	9 ± 1*	.001
Gastrocnemius medialis	24 ± 4.6	21 ± 2	.059
Soleus			
Superficial	56 ± 11	47 ± 7	.059
Deep	15 ± 3	12 ± 3	.153
Superficial posterior compartment of lower leg	106 ± 18	90 ± 11*	.022
Deep posterior compartment of lower leg†	40 ± 4	32 ± 6*	.004
All plantar flexor muscles (superficial posterior + deep posterior compartments of lower leg)	146 ± 19	122 ± 14*	.004
TQ (N · m)	142 ± 23	102 ± 16*	.001
Muscle moment arm length (m)	0.045 ± 0.002	0.042 ± 0.002*	.005
Muscle force (N)	3183 ± 511	2437 ± 334*	.001

Note.—Data are means ± standard deviation. PCSA = physiologic cross-sectional area, TQ = torque measured during maximal voluntary contraction.

* Significantly different from men.

† Deep posterior compartment of lower leg includes tibialis posterior, flexor digitorum longus, flexor hallucis longus, and popliteus.

The external torque and muscle volume assessed in our study were in the same range as those reported previously (3,29). Sex difference was found regarding both the maximal plantar flexion torque (38.8% for men) and the plantar flexor muscle volume (20.2% for men). One might wonder why the maximal plantar flexor torque difference was larger than the muscle volume difference. This discrepancy can be associated with a higher muscle moment arm previously reported in men (29), differences in mechanical properties of muscle-tendon tissues conditioning muscle tension transmission (29,30) and muscle structural organization (15,16). By using lower-field MR imaging (ie, 1.5 T), Galbán et al previously determined that men on average had higher muscle FA than did women (15). In our study, a higher FA was shown for the major part of lower leg muscle including the gastrocnemius lateralis in women compared with men, but no significant sex difference was observed for the gastrocnemius medialis and the soleus. The discrepancies in the results of the study by Galbán et al and our study can be linked to the experimental methodology (ie, a single-slice analysis in the study by Galbàn et al versus a large three-dimensional volume assessment in our study). This difference can partly explain the discrepancies inasmuch as our study illustrated that FA and/or MD could vary along the muscle length (as well as L_F and pennation angle). Therefore, the assessment of muscle diffusion properties and architecture should be preferred on a large muscle volume.

In our study, only slight sex differences were found regarding architecture on whole muscle. On the basis of US measurements, shorter muscle fascicle length and larger pennation angle have been reported in men compared with women (16). These apparent differences between results obtained with US and MR imaging might stem from the fact that hundreds of thousands of muscle fiber tracts were analyzed by using MR tractography in our study, whereas only tens of muscle fiber tracts, mainly located in the muscle belly, are analyzed on US images. The localization of the measure with US has a major impact on the analysis considering, for instance, the complex structural organization of the soleus (31).

Overall, MR imaging measurements illustrated a smaller muscle volume and a higher FA in women compared with men, whereas muscle architecture was comparable. The higher muscle FA value in women was related to concomitant nonsignificant changes in eigenvalues, leading to higher longitudinal diffusivity in women. On that basis, one might consider muscle fiber density as an accounting factor of the significant sex differences in D_F inasmuch as fiber cross-sectional area was found to be lower in women compared with men (32). In addition, a smaller fiber density has been reported in tibialis anterior of women compared with men (33), and this result is further supported by the result found for ACLL in our study. Although the physiologic meaning of D_F is not yet clear, it has to be emphasized that this is a reproducible index that can be measured noninvasively and potentially be used to indirectly assess relative cross-sectional area of muscle fibers and fascicles. However, further studies are needed to clarify the significance of D_F and its application to the assessment of skeletal muscle.

It has been previously suggested that investigation of diffusion properties of skeletal muscle might provide

Figure 6: Box plots show fractional anisotropy (FA) and mean diffusivity (MD) in distal (DIST), central (MID), and proximal (PROX) parts of lower leg muscles in men (blue) and women (red). Although significant differences were observed between men and women, additional differences were found independently of sex in FA and MD along several muscles of lower leg (flexor digitorum longus [FDL], flexor hallucis longus [FHL], gastrocnemius lateralis [GL], gastrocnemius medialis [GM], popliteus [POP], deep part of soleus [SO_{deep}], superficial part of soleus [SO_{sup}], tibialis posterior [TP], and muscles included in lateral component of lower leg [LCLL] and anterior component of lower leg [ACLL]). ∗ = significant difference between parts and sex (post hoc comparison from length × sex interaction effect). † = significant difference between parts (post hoc comparison from length main effect).

Figure 7

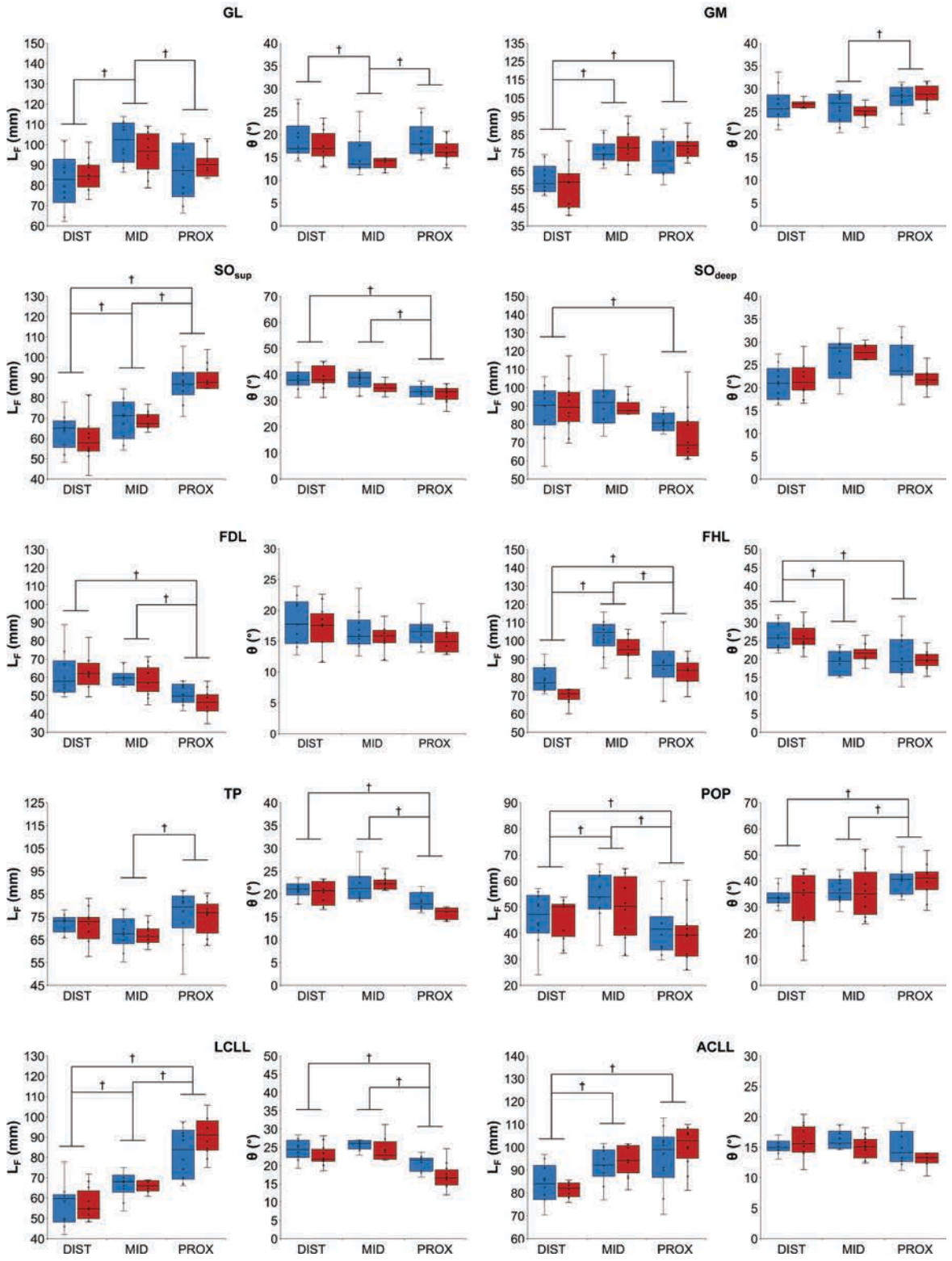
GL
GM
SO$_{sup}$
SO$_{deep}$
FDL
FHL
TP
POP
LCLL
ACLL
L$_F$ (mm)
θ (°)
DIST
MID
PROX
†

Figure 8

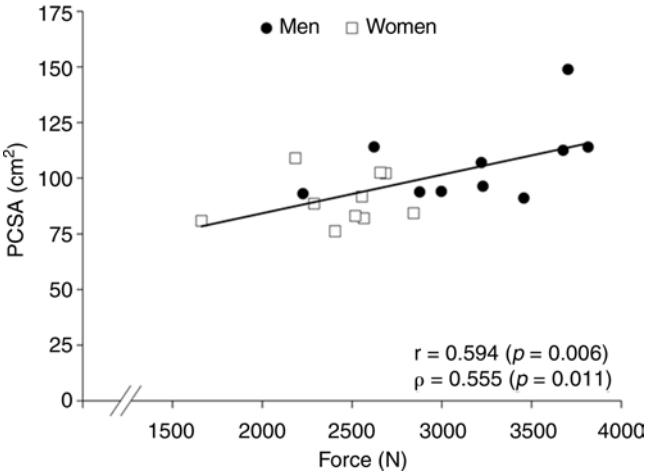

Figure 8: Graph shows correlation between maximal muscle force and physiologic cross-sectional area (PCSA) of superficial posterior compartment of lower leg (SPCLL) in men (full circles) and women (empty squares).

relevant indexes for the evaluation of skeletal muscle integrity in physiologic and pathophysiologic situations (34). Considering the positive correlation between the PCSA of the main plantar flexor muscles and the maximal isometric muscle force reported in our study, one might consider that ultra-high-field-strength MR imaging and the corresponding PCSA measurement at rest could be used as a reliable, noninvasive method of quantifying the expected maximal muscle force production capacity in vivo. Clinical assessment of individual muscles relative contribution to muscle force production might also be of interest in the context of specific and localized alteration of muscle tissue, as shown in several muscular diseases (35).

Our study had several limitations. Sample sizes were relatively small and the interobserver reproducibility was not assessed. However, the low interindividual variability, the power analysis, and the good reproducibility of diffusion and architecture parameters significantly supported our results. Our study was conducted in healthy young participants and one can question the feasibility in patients with fat infiltration (35). Although potential error in direction of principal diffusion can occur as a result of fat infiltration (14), this effect can be limited with an effective fat-suppression technique (6). It is noteworthy that fat infiltration would have no effect on the segmentation and registration strategy we used as previously indicated (24). From a technical point of view, the acquisition time could be reduced with the implementation of multiband developments to the DTI sequence (eg, 36). In addition, parameters (eg, number of directions, *b* values) could be further optimized to marginally increase the quality of diffusion-weighted images.

In conclusion, high-spatial-resolution DTI obtained at ultra-high-field-strength allows an accurate and reproducible quantification of structural organization of skeletal muscle fibers. This application of ultra-high-field-strength MR imaging might be of high interest for the assessment of muscular injuries in both athletes and patients with muscular disorders. In that context, the corresponding impact on muscle function and the potential effects of clinical intervention could be investigated.

Acknowledgments: The authors thank the Assistance Publique des Hôpitaux de Marseille (APHM), the Centre National de la Recherche Scientifique (CNRS UMR 7339), and all the participants who participated in this study.

Disclosures of Conflicts of Interest: A.F. disclosed no relevant relationships. **A.C.O.** disclosed no relevant relationships. **A.L.T.** disclosed no relevant relationships. **C. V.** disclosed no relevant relationships. **T.F.** Activities related to the present article: disclosed no relevant relationships. Activities not related to the present article: disclosed no relevant relationships. Other relationships: is an employee and shareholder of Siemens; holds patents filed by Siemens. **M.G.** disclosed no relevant relationships. **J.G.** disclosed no relevant relationships. **P.B.** disclosed no relevant relationships. **D.B.** disclosed no relevant relationships.

References

1. Godi C, Ambrosi A, Nicastro F, et al. Longitudinal MRI quantification of muscle degeneration in Duchenne muscular dystrophy. Ann Clin Transl Neurol 2016;3(8):607–622.
2. Lieber RL, Fridén J. Clinical significance of skeletal muscle architecture. Clin Orthop Relat Res 2001 (383):140–151.
3. Fukunaga T, Roy RR, Shellock FG, Hodgson JA, Edgerton VR. Specific tension of human plantar flexors and dorsiflexors. J Appl Physiol (1985) 1996;80(1):158–165.
4. Lieber RL, Fridén J. Functional and clinical significance of skeletal muscle architecture. Muscle Nerve 2000;23(11):1647–1666.
5. Maganaris CN, Baltzopoulos V, Sargeant AJ. In vivo measurements of the triceps surae complex architecture in man: implications for muscle function. J Physiol 1998;512(Pt 2):603–614.

Figure 7: Box plots show fiber length (L_F) and pennation angle (θ) in distal (DIST), central (MID), and proximal (PROX) parts of lower leg muscles in men (blue) and women (red). Only a few significant sex differences were observed between men and women whereas, independently of sex, L_F and θ were altered along muscles (gastrocnemius medialis [GM], gastrocnemius lateralis [GL], deep part of soleus [SO_{deep}], superficial part of soleus [SO_{sup}], flexor hallucis longus [FHL], flexor digitorum longus [FDL], tibialis posterior [TP], popliteus [POP], and muscles included in lateral compartment of lower leg [LCLL] and anterior compartment of lower leg [ACLL]). ∗ = significant difference between parts and sex (post hoc comparison from length × sex interaction effect). † = significant difference between parts (post hoc comparison from length main effect).

6. Damon BM, Froeling M, Buck AK, et al. Skeletal muscle diffusion tensor-MRI fiber tracking: rationale, data acquisition and analysis methods, applications and future directions. NMR Biomed 2017;30(3):e3563.
7. Fouré A, Duhamel G, Wegrzyk J, et al. Heterogeneity of muscle damage induced by electrostimulation: a multimodal MRI study. Med Sci Sports Exerc 2015;47(1): 166–175.
8. McMillan AB, Shi D, Pratt SJ, Lovering RM. Diffusion tensor MRI to assess damage in healthy and dystrophic skeletal muscle after lengthening contractions. J Biomed Biotechnol 2011;2011:970726.
9. Sinha U, Csapo R, Malis V, Xue Y, Sinha S. Age-related differences in diffusion tensor indices and fiber architecture in the medial and lateral gastrocnemius. J Magn Reson Imaging 2015;41(4):941–953.
10. Heemskerk AM, Sinha TK, Wilson KJ, Ding Z, Damon BM. Quantitative assessment of DTI-based muscle fiber tracking and optimal tracking parameters. Magn Reson Med 2009;61(2):467–472.
11. Budzik JF, Le Thuc V, Demondion X, Morel M, Chechin D, Cotten A. In vivo MR tractography of thigh muscles using diffusion imaging: initial results. Eur Radiol 2007;17(12):3079–3085.
12. Heemskerk AM, Sinha TK, Wilson KJ, Ding Z, Damon BM. Repeatability of DTI-based skeletal muscle fiber tracking. NMR Biomed 2010;23(3):294–303.
13. Froeling M, Oudeman J, van den Berg S, et al. Reproducibility of diffusion tensor imaging in human forearm muscles at 3.0 T in a clinical setting. Magn Reson Med 2010;64(4):1182–1190.
14. Damon BM. Effects of image noise in muscle diffusion tensor (DT)-MRI assessed using numerical simulations. Magn Reson Med 2008;60(4):934–944.
15. Galbán CJ, Maderwald S, Uffmann K, Ladd ME. A diffusion tensor imaging analysis of gender differences in water diffusivity within human skeletal muscle. NMR Biomed 2005;18(8):489–498.
16. Chow RS, Medri MK, Martin DC, Leekam RN, Agur AM, McKee NH. Sonographic studies of human soleus and gastrocnemius muscle architecture: gender variability. Eur J Appl Physiol 2000;82(3):236–244.
17. Stejskal EO, Tanner JE. Spin diffusion measurements: spin echoes in the presence of a time dependent field gradient. J Chem Phys 1965;42(1):288–292.
18. Park HW, Kim DJ, Cho ZH. Gradient reversal technique and its applications to chemical-shift-related NMR imaging. Magn Reson Med 1987;4(6):526–536.
19. Holland D, Kuperman JM, Dale AM. Efficient correction of inhomogeneous static magnetic field-induced distortion in echo planar imaging. Neuroimage 2010;50(1):175–183.
20. Ogier A, Sdika M, Fouré A, Le Troter A, Bendahan D. Individual muscle segmentation in MR images: a 3D propagation through 2D non-linear registration approaches. Conf Proc IEEE Eng Med Biol Soc 2017;2017:317–320.
21. Maggioni M, Katkovnik V, Egiazarian K, Foi A. Nonlocal transform-domain filter for volumetric data denoising and reconstruction. IEEE Trans Image Process 2013;22(1):119–133.
22. Tustison NJ, Avants BB, Cook PA, et al. N4ITK: improved N3 bias correction. IEEE Trans Med Imaging 2010;29(6):1310–1320.
23. Calamante F. Track-weighted imaging methods: extracting information from a streamlines tractogram. MAGMA 2017; 30(4):317–335.
24. Fouré A, Le Troter A, Guye M, Mattei JP, Bendahan D, Gondin J. Localization and quantification of intramuscular damage using statistical parametric mapping and skeletal muscle parcellation. Sci Rep 2015;5(1): 18580.
25. Sigmund EE, Vivier PH, Sui D, et al. Intravoxel incoherent motion and diffusion-tensor imaging in renal tissue under hydration and furosemide flow challenges. Radiology 2012;263(3):758–769.
26. Fouré A, Nordez A, McNair P, Cornu C. Effects of plyometric training on both active and passive parts of the plantarflexors series elastic component stiffness of muscle-tendon complex. Eur J Appl Physiol 2011;111(3):539–548.
27. Lee SS, Piazza SJ. Built for speed: musculoskeletal structure and sprinting ability. J Exp Biol 2009;212(Pt 22):3700–3707.
28. Wickiewicz TL, Roy RR, Powell PL, Edgerton VR. Muscle architecture of the human lower limb. Clin Orthop Relat Res 1983 (179):275–283.
29. Fouré A, Cornu C, McNair PJ, Nordez A. Gender differences in both active and passive parts of the plantar flexors series elastic component stiffness and geometrical parameters of the muscle-tendon complex. J Orthop Res 2012;30(5):707–712.
30. Souron R, Bordat F, Farabet A, et al. Sex differences in active tibialis anterior stiffness evaluated using supersonic shear imaging. J Biomech 2016;49(14):3534–3537.
31. Agur AM, Ng-Thow-Hing V, Ball KA, Fiume E, McKee NH. Documentation and three-dimensional modelling of human soleus muscle architecture. Clin Anat 2003;16(4): 285–293.
32. Simoneau JA, Bouchard C. Human variation in skeletal muscle fiber-type proportion and enzyme activities. Am J Physiol 1989;257(4 Pt 1):E567–E572.
33. Porter MM, Stuart S, Boij M, Lexell J. Capillary supply of the tibialis anterior muscle in young, healthy, and moderately active men and women. J Appl Physiol (1985) 2002;92(4): 1451–1457.
34. Budzik JF, Balbi V, Verclytte S, Pansini V, Le Thuc V, Cotten A. Diffusion tensor imaging in musculoskeletal disorders. RadioGraphics 2014;34(3):E56–E72.
35. Lareau-Trudel E, Le Troter A, Ghattas B, et al. Muscle quantitative MR imaging and clustering analysis in patients with facioscapulohumeral muscular dystrophy type 1. PLoS One 2015;10(7):e0132717.
36. Wen Q, Kelley DA, Banerjee S, et al. Clinically feasible NODDI characterization of glioma using multiband EPI at 7 T. Neuroimage Clin 2015;9:291–299 .